JOURNAL OF MATERIALS SCIENCE 23 (1988) 1309–1316

Electron microscopy of internally reduced (Mg, Ni)O

M. BACKHAUS-RICOULT, D. RICOULT*
Institut für Physikalische Chemie und Elektrochemie, Universität Hannover, Callinstr. 3-3a, D 3000 Hannover, FRG

(Mg, Ni)O single crystals were internally reduced at 1273 and 1673 K in graphite ampules. As a result, discrete nickel precipitates developed inside the MgO matrix. The precipitates, as well as the dislocations that surround them, and the pores have been observed by means of electron microscopy. A model is proposed, whereby the morphology of the metal precipitates is controlled by the kinetics and the mechanism of internal reduction. The interactions between point defects and dislocations or pores are also commented upon.

1. Introduction

Internal reactions occurring in metal alloys or in non-metal systems have been thoroughly described by Wagner [1] and by Schmalzried [2, 3]. To provide the necessary background for the present work, only a brief review of the model proposed by these authors will be presented here. Furthermore, only the case of the internal reduction of an (Mg, Me)O mixed oxide (Me = Co, Ni, Fe, . . .), which is of particular relevance to our purpose, will be considered. As shown in the schematic diagram of Fig. 1, a change in the oxygen pressure surrounding the crystal of a mixed oxide solid solution (Mg, Me)O from a starting equilibrium condition a''_{O_2} to a lower value a'_{O_2} results, after equilibration of the material to this new condition, in the precipitation of the more noble metal Me, which is then in thermodynamically stable coexistence with the metal-depleted oxide. If the reduction occurs as an external reaction, a continuous metal layer of Me forms at the outer surface. On the other hand, if the reaction occurs internally, discrete metal precipitates form inside the ceramic matrix. If the concentration of Me in the starting mixed oxide is low, and if the newly formed precipitates do not influence the transport properties of the matrix, the overall reaction can be interpreted in terms of cation diffusion from the surface towards the bulk of the specimen and of simultaneous diffusion of cation vacancies and electron holes towards the surface (Fig. 2). This formal description of internal reduction does not involve any long-range transport of oxygen. However, since large metal precipitates do form inside the oxide lattice, the oxygen sublattice must be locally disrupted in order to provide the free volume necessary for the growth of the new phase.

The kinetics of the reduction of (Mg, Me)O with Me = Fe, Co, Ni have already been extensively studied [4, 5], especially with respect to the influence of cation (Me) concentration, temperature, reaction time and Me concentration homogeneity. In the previous investigations the morphological variability of the metal–ceramic composites thus formed has been emphasized and qualitatively analysed in terms of transport kinetics. In particular, it has been proposed that the morphology of the composite is determined by two factors: (a) whether oxygen or cation transport is faster, and (b) whether diffusion takes place through the oxide bulk, along dislocations in the oxide lattice, through metal precipitates, or along metal–ceramic interfaces. The parameters investigated (temperature, Me concentration, Me concentration gradient and oxygen activity at the sample surface) are indeed likely to strongly affect the diffusion kinetics.

It is the purpose of this paper to contribute to the investigation of the atomistic mechanisms taking place during the course of internal reduction, by means of electron microscopy. The system selected for this study is (Mg, Ni)O.

2. Experimental procedure

Slices of MgO single crystals (Spicer, England) were embedded in NiO powder and annealed at 1973 K in air for 72 h, at the end of which the powder was removed. The crystal slices were then further annealed at the same temperature for up to 10 days, in order to homogenize the nickel concentration. Electron microprobe analyses showed that the crystals investigated were not homogeneous. Rather, the nickel concentration was about 30 cation % at the surface and dropped to zero at depths of 200 to 300 μm (see [5]). The samples were then reduced in graphite ampoules at 1673 K for 8 h (Type 1 specimen) or at 1273 K for three days (Type 2 specimen). The oxygen activity in the ampoule corresponds roughly to the C/CO buffer established by the ampoule material at the reaction temperature (10^{-18} at 1673 K and 10^{-21} at 1273 K). Specimens of both types were cut perpendicularly to their outer surface for scanning electron microscope (SEM) investigations. For transmission electron microscopy (TEM) studies, other slabs, cut parallel to the

* *Present address:* Corning Europe, 7 bis Avenue de Valvins, F-77210 Avon, France. (Reprints should be ordered from this address.)

0022–2461/88 $03.00 + .12

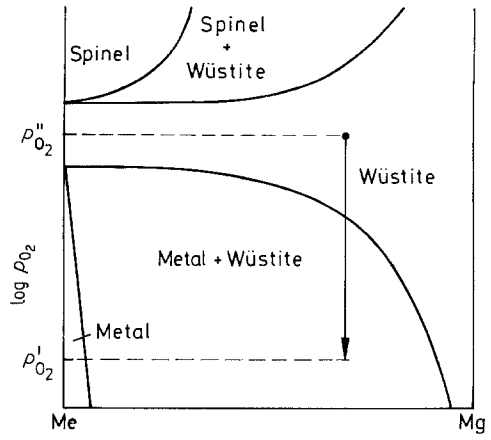

Figure 1 Schematic phase diagram of the second kind for the system Mg–Me–O where Me = Ni, Co, Fe . . . .

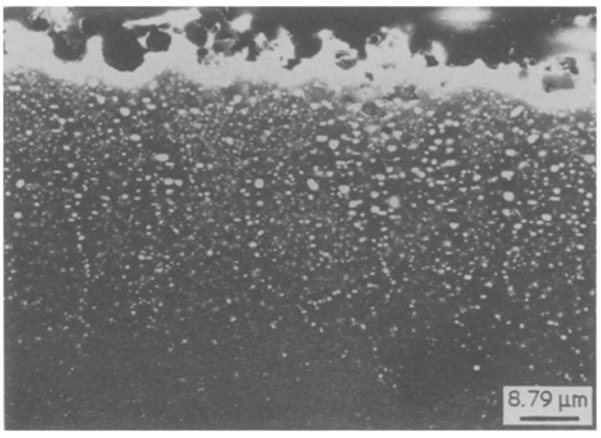

Figure 3 SEM micrograph of a sample reduced at 1673 K in a graphite ampoule.

reacted surface, were mechanically thinned and polished with diamond paste to a thicnkess of 40 μm, before being further ion-milled (argon bombardment) until perforation was visible. Such thin films were always prepared in such a way that the transparent region (i.e. the thinnest region close to the hole) was located in the reaction layer. As a result of the preferential thinning of the metal phase, the nickel precipitates were preferentially etched. In some instances, larger nickel precipitates were even thinned away, leaving a hole, whereas the ceramic matrix was still quite thick. As a consequence, the thinning process always resulted in samples of a very inhomogeneous thickness.

The microscopes used for this investigation were a scanning electron microscope (B & L, Nanolab 2100) and transmission electron microscopes (Jeol 200CX operated in TEM and STEM (scanning transmission electron microscopy) modes at 200 kV, equipped with an energy-dispersive analytical system (EDX); Jeol 1200 operated in TEM mode at 120 kV; and Siemens Elmiscope 102 operated at 125 kV).

3. Results

Typical SEM micrographs of reduced samples of Types 1 and 2 are shown in Figs 3 and 4. In the inhomogeneous samples reduced at 1673 K (Type 1) randomly distributed precipitates of average size 1 μm are visible close to the outer surface. No preferential orientation between second-phase particles and matrix can be detected on this scale. Further away from the surface, the precipitates become aligned either perpendicularly to the outer surface, or sometimes even parallel to it. In this layer, numerous pores may be seen which appear to have grown like channels from the outer surface, which as a result has evolved into a non-planar, porous surface.

The samples of Type 2, which were reduced at the lower temperature (1273 K) reveal a very different morphology (Fig. 4). The reduction seems to have occured inhomogeneously: tree-like structures consisting of metal particles and pores have grown from the surface into the bulk of the samples, while the material between the "trees" does not show any sign of reduction at the scale of observation (SEM).

Transmission electron microscopy provides a very valuable complement of information. The thin foils were prepared in the way described above, so that they would be transparent to the electron beam in a region of the reduced layer located about 20 to 30 μm away from the original outer surface. In Fig. 5a a typical thin area of a Type 1 sample is shown. The precipitates are randomly distributed and vary in size from a few nanometres to 1 μm. STEM EDX analyses of the

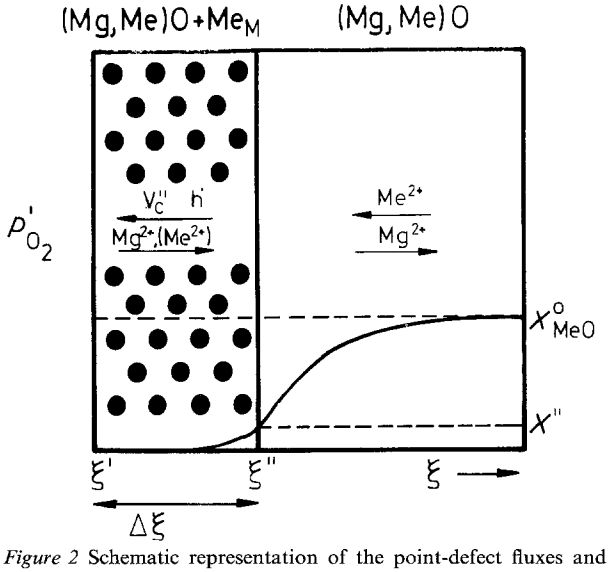

Figure 2 Schematic representation of the point-defect fluxes and precipitate formation occurring during the internal reduction of a mixed oxide (Mg, Me)O. At ξ', "MgO" + V_c'' + 2h· = Mg_c^x + $\frac{1}{2}O_2$; at ξ'', Me_c^x = Me_M + V_c'' + 2h·.

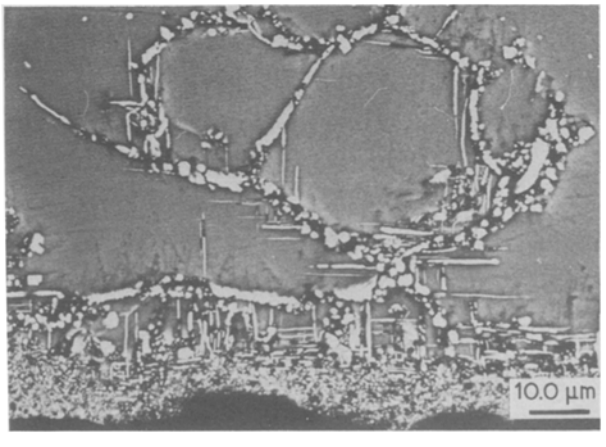

Figure 4 SEM micrograph of a sample reduced at 1273 K in a graphite ampoule.

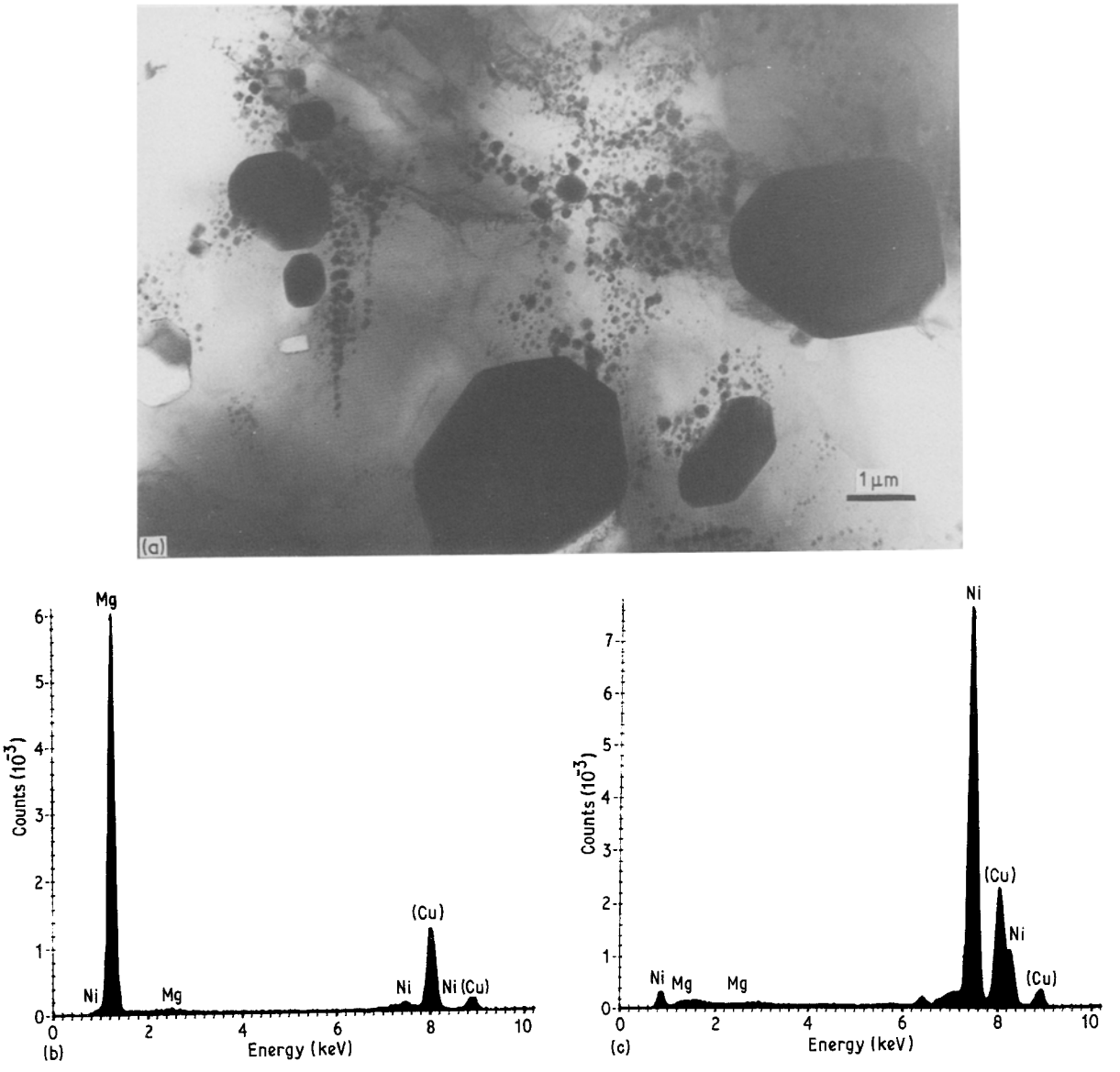

Figure 5 (a) Bright-field image (TEM) of a typical region of the reaction layer formed during Type 1 reduction treatment (see text). Spectra of (b) the pure matrix and (c) a metal precipitate.

precipitates of various sizes and of the matrix between the precipitates prove that the coexisting phases of the composite are really MgO and nickel (Figs 5b and c). The small copper peak visible in the spectra is due to the copper grid which was used to support the specimens in the microscope holder. For smaller precipitates and areas close to an interface, the smallest available probe size of the microscope (Jeol 200CX), 3.5 nm, was used, which yields information over an area of ≈ 10 nm diameter for a sample thickness of about 120 nm. In these conditions of analysis, we found that in all cases (even at very high nickel content in the starting mixed oxide) the reduced oxide matrix located between the precipitates was always totally depleted in nickel after the reduction. At first, this observation seems to contradict the measurements presented by Ricoult and Schmalzreid [4], where it was stated that the matrix depletion between the precipitates was not complete in the reduced samples initially containing the most nickel. However, this statement relied only on EDX measurements performed on bulk specimens in a scanning microscope, in which the best spatial analytical resolution is not better than 1 μm. The higher image resolution obtained by transmission electron microscopy (Fig. 5) also reveals the presence of many smaller precipitates, only a few hundreds of nanometres apart from each other. Although they could not be imaged in the SEM, they are certainly responsible for the finite nickel concentration measured in the reduced oxide matrix by this technique.

All nickel precipitates are found to be topotactically oriented with respect to the matrix, so that every crystallographic plane of the precipitate is parallel to the corresponding plane of the oxide:

$$[1\,0\,0]_{MgO} \parallel [1\,0\,0]_{Ni} \quad \text{and} \quad (0\,0\,1)_{MgO} \parallel (0\,0\,1)_{Ni}$$

Selected-area diffraction patterns (SAD) taken at the matrix–precipitate interface are shown in Fig. 6 for two orientations of the electron beam with respect to the crystal. In addition to the normal reflections of the nickel and MgO lattices, many other reflections with a high symmetry are also visible, which are ascribed to double diffraction. The exact topotactic alignment of the two phases was verified by microdiffraction techniques. Convergent-beam electron diffraction patterns of interface areas show no tilt or shift between the symmetry elements of the characteristic patterns of the two phases. Furthermore, this observation is

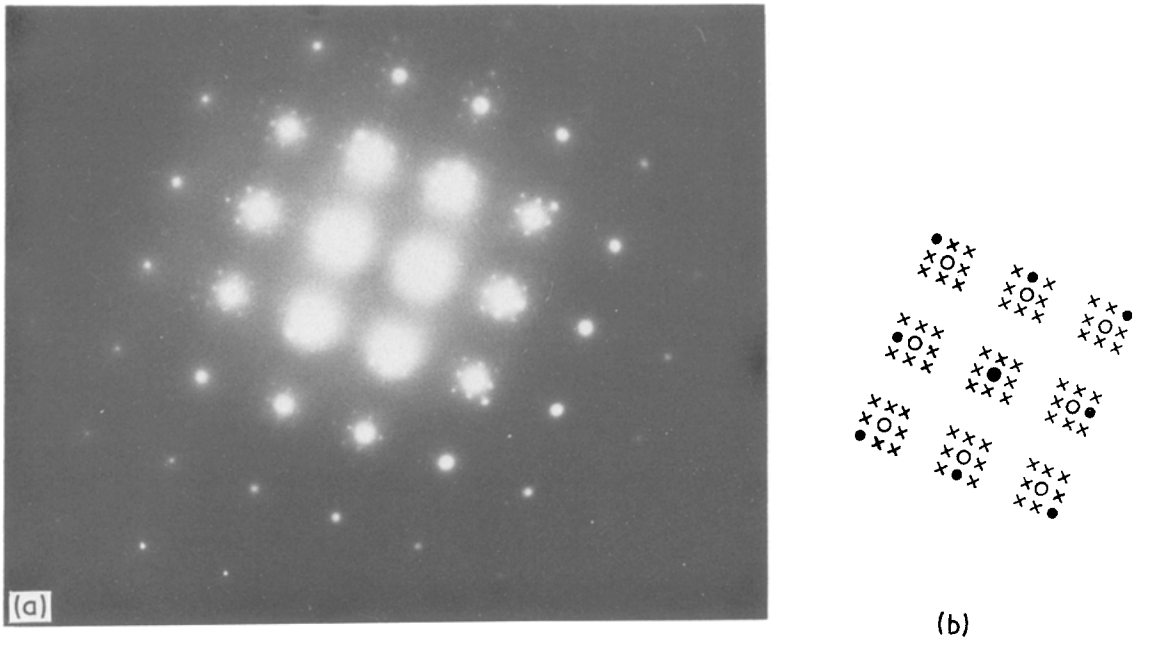

Figure 6 (a) Selected-area diffraction pattern demonstrating the orientation relationship between matrix and metal precipitates: $[1\,0\,0]_{MgO} \parallel [1\,0\,0]_{Ni}$, $(0\,1\,0)_{MgO} \parallel (0\,1\,0)_{Ni}$. (b) Key to (a): (○)MgO reflections, (●) nickel, (x) double diffraction.

independent of the size of the precipitates (10 nm to 1 μm).

Fig. 5 is a typical example of the very irregular size distribution of the precipitates, ranging from a few nanometres to about 1 μm. From such image observations, the size and the morphology of the precipitates can be correlated. Large precipitates (300 nm to 1 μm) are cube-shaped, with rounded corners. The large faces are always $\{0\,0\,1\}$ planes, while the faces forming the rounded corners are planes of the $\{1\,1\,0\}$ type. Smaller particles (100 to 300 nm) are more or less regular polyhedra (viewed along the $\langle 1\,0\,0\rangle$ direction, they look like regular hexagons), faces of which being again $\{1\,0\,0\}$ and $\{1\,1\,0\}$. Finally, the tiny precipitates are cube-shaped, with only $\{1\,1\,0\}$ or $\{1\,0\,0\}$ faces. Pores, sometimes visible in the matrix, show the typical faceting of MgO in $\{0\,0\,1\}$ planes.

These observations hold for distances up to 25 μm away from the outer surface, but at larger distances, areas can sometimes be found in the TEM which contain a high density of very regularly distributed precipitates (Fig. 7). Both the size and the morphology of these precipitates are homogeneous. These zones of precipitate were also observed in other work [5] and described as "pockets" of precipitates. In some submicrometer scale observations, an alignment of small precipitates (diameter close to 25 nm) in rows could be detected (Fig. 7), the main orientations of which were along the $\langle 1\,0\,0\rangle$ directions of the MgO crystal.

Samples of Type 2 with the same starting nickel concentration profile as those of Type 1 yield, after the reduction at lower temperature, exactly the same orientation relationship between particles and matrix (SAD pattern of Fig. 8b). However, the precipitates located between the tree-like metal/pore structures observed by SEM (see description above) have a very different morphology (Fig. 8a). The precipitates are much smaller, their size ranging from 2 nm × 2 nm × 2 nm to 10 nm × 10 nm × 50 nm, and are bar-shaped with $\{1\,1\,0\}$ faces. These small precipitates are quite regularly distributed over the whole thin area and, of course, could not be detected by the previous SEM investigations.

A typical dislocation structure was also observed in Type 2 samples (Fig. 8). The only dislocations detected were small loops encircling a few precipitates or more rarely, larger loops enclosing a higher density

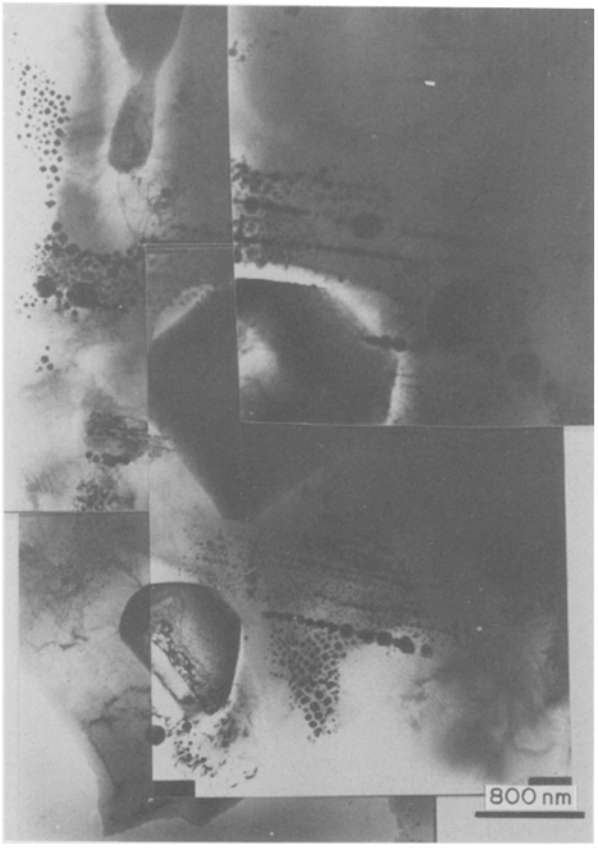

Figure 7 TEM bright-field image showing aligned precipitates, as well as the high density of small precipitates after a reduction of Type 1.

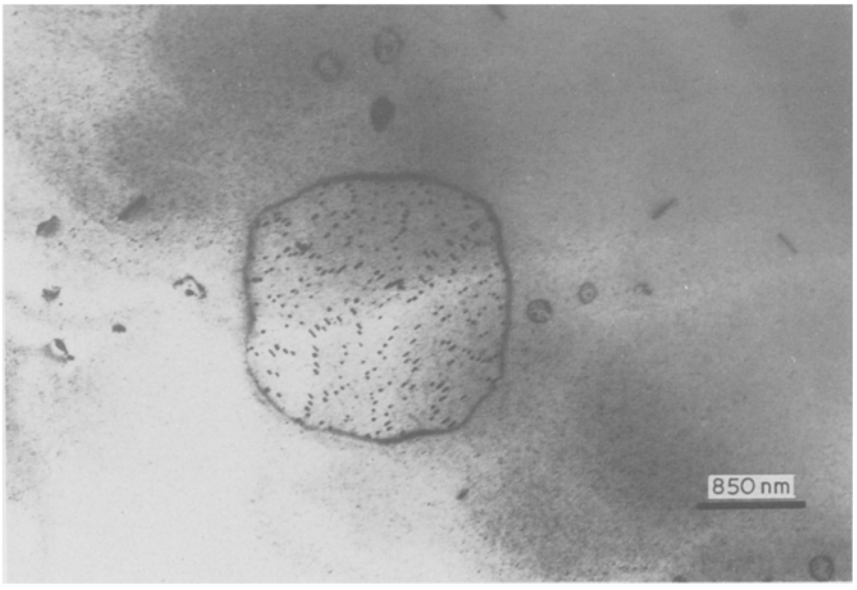

Figure 8 TEM bright-field image of a typical region of the reaction layer formed during internal reduction of (Mg, Ni)O (Type 2).

of precipitates. The precipitates located inside the loops are larger by a factor of three than those outside the loops. This dislocation structure was observed between the tree-like metal features of Fig. 4. Due to their porosity and to the different thinning rates of metal and oxide, the preparation of a suitable thin film of the tree-like precipitation was not possible. However, due to the large size of the precipitates, a very different dislocation structure would be expected there, probably similar to the dislocations observed in Type 1 samples, where pores and larger precipitates were also present.

During the reduction, Type 1 specimens develop a dense dislocation network connecting the precipitates, as shown in Fig. 9. Even the smallest precipitate is connected to a larger one by at least one dislocation, like a string (Fig. 10). Due to the very high dislocation density, no Burgers vector analysis has been done. Every precipitate has to be surrounded by an array of misfit dislocations, in order to accommodate the large mismatch existing between the metal and the oxide lattices (17.6% misfit: $d_{MgO} = 0.421$ nm and $d_{Ni} = 0.352$ nm). The calculated distance between misfit dislocations is 1.6 nm. For the technical reasons evoked above, it was not possible to prepare a very thin interface area suitable for the observation of the interface dislocations by high-resolution electron microscopy.

It was possible to resolve moiré fringes due to the overlapping of the nickel precipitates and the oxide matrix. The moiré spacing experimentally observed for the 2 0 0 reflection is 1.18 nm, which is in very good agreement with the theoretically expected value of 1.13 nm (Fig. 11).

4. Discussion

The results of our STEM analysis show that even for high nickel concentrations in the starting mixed oxide, the matrix is completely depleted in the more noble metal after the reduction. These results are in agreement with the phase diagram and show that the depletion does obey the equilibrium thermodynamics. Before discussing the orientation relationship between matrix and precipitates which we found in our experiments, we would like to summarize the results of other investigations describing either similar reactions, or interesting phenomena of relevance to interface formation. The epitaxial growth of nickel on MgO

Figure 9 TEM bright-field image of a typical area in a reduced sample of Type 1. The dark lines are free dislocations in the MgO matrix. The bar is 1.1 μm.

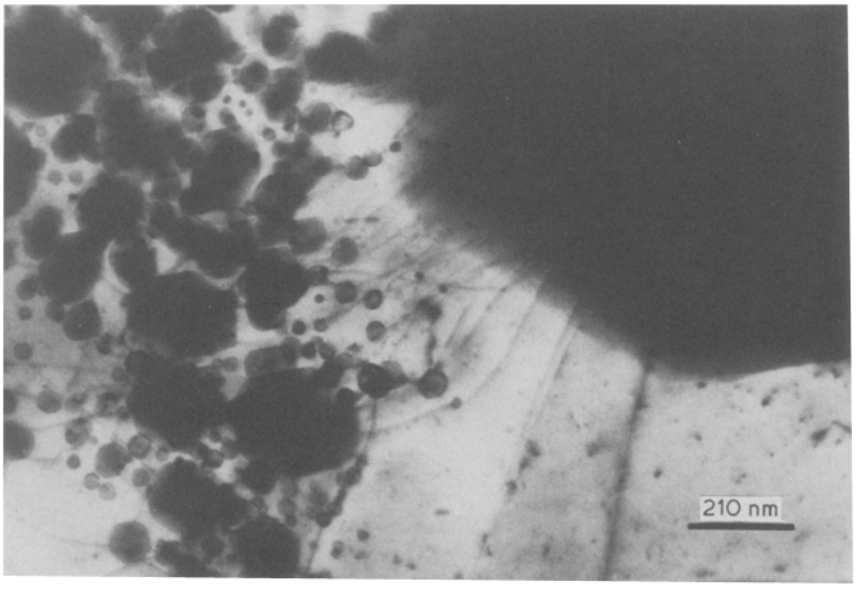

Figure 10 TEM bright-field image showing the interconnection of metal precipitates by dislocations after reduction of Type 1.

surfaces is well characterized in the overview by Honjo and Yagi [6]: the major orientation relationship between the two phases is $[0\,0\,1]_{MgO} \parallel [1\,\bar{1}\,2]_{Ni}$ and $(0\,0\,1)_{MgO} \parallel (1\,1\,\bar{1})_{Ni}$, while the relationship $[0\,0\,1]_{MgO} \parallel [0\,0\,1]_{Ni}$ and $(1\,0\,0)_{MgO} \parallel (1\,0\,0)_{Ni}$ occurs less often. This difference in occurrence of the two orientation relationships can easily be explained by the quality of the fit of the metal and oxide lattice planes, which is much better for the first orientation relationship (lattice mismatch = 2.5 to 3%) than for the second one (mismatch = 17.6%). In consequence, the growth of nickel on MgO: $[0\,0\,1]_{MgO} \parallel [0\,0\,1]_{Ni}$ and $(1\,0\,0)_{MgO} \parallel (1\,0\,0)_{Ni}$ does not yield a low-energy configuration. Even though these observations cannot be directly applied to our experiments, where precipitation occurs in the bulk (three-dimensional fit of the lattice planes), it is surprising that we find exclusively the orientation relationship leading to the higher mismatch, in our samples of both Type 1 and Type 2. Within 50 to 100 precipitates, not a single exception to this rule could be detected.

Relevant observations have also been made during the formation of nickel particles, either at the surface of NiO single crystals reduced during ion-milling [7], or at surfaces of NiO and (Mg, Ni)O powders reduced by electron irradiation in the TEM [8]. In both cases it was found that the metal would grow topotactically on the oxide phase, so that $[0\,0\,1]_{MgO} \parallel [0\,0\,1]_{Ni}$ and $(1\,0\,0)_{MgO} \parallel (1\,0\,0)_{Ni}$.

Different results were reported by Narayan and co-workers [9, 10], who reduced (Mg, Ni)O single crystals (0.1 to 0.5 at % Ni) at 1450 K in graphite, or at 2100 K in magnesium vapour. Even though the precipitates formed during the heat-treatments are similar in size and morphology to those found in our samples, they differ in their major orientation relationship with the matrix. In the samples reduced at lower temperatures these authors find $(1\,0\,0)_{MgO} \parallel (1\,\bar{1}\,2)_{Ni}$ and $(0\,1\,0)_{MgO} \parallel (\bar{1}\,1\,1)_{Ni}$, and they also mention that the percentage of particles aligned in such a way that $[0\,0\,1]_{MgO} \parallel [0\,0\,1]_{Ni}$ and $(1\,0\,0)_{MgO} \parallel (1\,0\,0)_{Ni}$ increases with temperature and time, to finally reach 100% at 2100 K and 7 h. Assuming that the lattice mismatch between the two phases gives the main contribution to the energy of the system, then these results could be interpreted as suggesting that the energetically favoured orientation relationship, $(0\,0\,1)_{MgO} \parallel (1\,\bar{1}\,2)_{Ni}$ and $(1\,0\,0)_{MgO} \parallel (\bar{1}\,1\,1)_{Ni}$, forms first (smaller

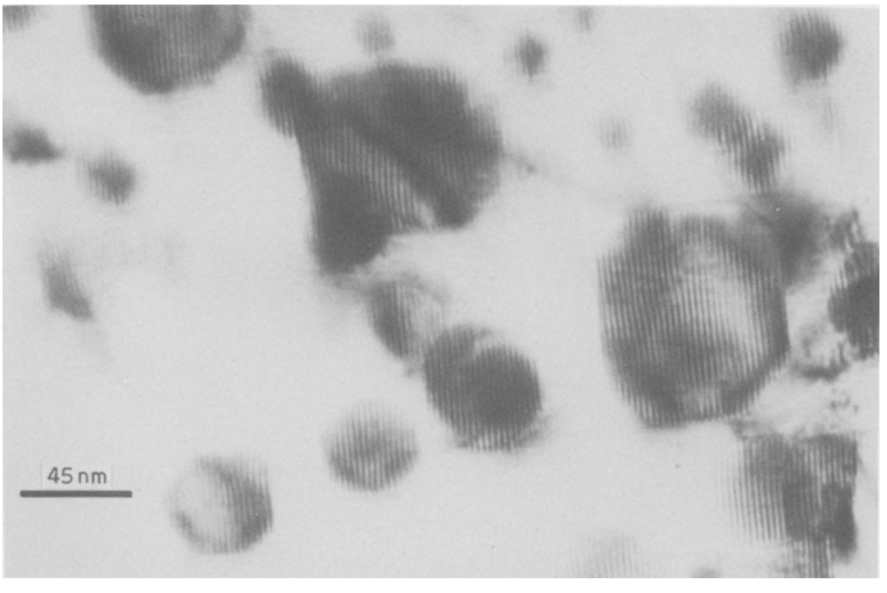

Figure 11 Moiré fringes due to the overlap of nickel precipitates and MgO matrix, representative of the mismatch between the two lattices.

mismatch),and then transforms to $[0\,0\,1]_{MgO} \parallel [0\,0\,1]_{Ni}$ and $(1\,0\,0)_{MgO} \parallel (1\,0\,0)_{Ni}$ during the reaction at high temperature, where thermal energy renders the larger misfit permissible. However, this interpretation would seem dubious to us: why would an energetically unfavourable orientation relationship develop out of a lower-energy one? We propose that the interface formation is not only controlled by the thermodynamics (energy considerations), but is also influenced by the kinetics of internal reduction. The process of particle formation and growth during internal reduction of the mixed oxide (Mg, Ni)O will be analysed in these terms in the following.

To understand how reaction kinetics can influence the final precipitate morphology, it is useful to focus on the atomistic aspects of metal formation in the oxide lattice, which can be described by the reaction

$$Ni_{cat}^{x} = Ni_{me} + V_{cat}'' + 2h^{\cdot} \quad (1)$$

where "cat" and "me" refer to cationic and metal sites, respectively, the superscript^{x} refers to a neutral charge (with respect to the normal point lattice charge), V'' are doubly charged vacancies and $h^{\cdot}$ are electron holes. At first, metal clusters form and grow to a critical size where they become energetically stable nuclei. At this early stage, the nuclei are still coherent with the surrounding oxide lattice. However, due to the difference between the lattice constants of the two phases, a strong strain field develops around the precipitates, as well as a local increase of the MgO chemical potential under the local stress field. Due to the slow oxygen diffusion in MgO, it is not possible to relax this potential by outward diffusion of MgO lattice molecules. At a more advanced stage of the growth process, the particles become incoherent and an array of misfit dislocations accommodating the lattice mismatch forms at the boundaries. Equation 1 shows clearly that for every metallic nickel atom precipitated, one vacancy in the cationic sublattice is created, which must disappear at this locus in order to reestablish the local point-defect equilibrium. Various possibilities for the outward vacancy transport or vacancy annihilation exist:

(i) bulk diffusion of cation vacancies towards the surface,

(ii) pipe diffusion of cation vacancies along dislocations,

(iii) collapse of vacancy pairs leading to loop formation, and

(iv) diffusion towards dislocations which act as vacancy sinks and then climb.

In general, only the first possibility is envisioned in the literature: it corresponds to the simplified ideal case of a perfect single crystal, where thermodynamic equilibrium is established everywhere in the crystal. However, in real crystals linear defects are present, namely, dislocations can act as short-circuit paths to the surface. The last two possibilities (loop formation and climb of dislocations), although they can reasonably account for vacancy annihilation in metals, have to be carefully analysed in the case of ionic crystals. In both cases, diffusion of both cation and oxygen vacancies is required in order to keep the MgO structure at the dislocation. In local thermodynamic equilibrium, the oxygen vacancy concentration is negligible in MgO; therefore the necessary point-defect pairs (cation vacancy and oxygen vacancy) are not in a sufficient number to allow these processes to take place. As soon as the local thermodynamic equilibrium is disturbed, mechanisms (iii) and (iv) can however be considered as being possible.

After having discussed the diffusion of the cation vacancies, let us now focus on the outward diffusion of oxygen. It is intuitively clear that in order for metal to precipitate inside an oxide lattice, oxygen must also locally disappear [4, 11]. At a dislocation or a pore, Equation 1 can be rewritten in the following way:

$$Ni_{cat}^{x} + O_{an}^{x} \rightarrow Ni_{me}^{x} + V_{cat}'' + V_{an}^{x} + 2h^{\cdot} + O\uparrow \quad (2)$$

where the subscript "an" stands for the anion lattice sites in the oxide lattice. From this formulation a vacancy pair, corresponding to a missing lattice molecule in the oxide phase, can be formed when the possibility for an outward diffusion of oxygen along short-circuit paths (dislocations or pore arrays) exists. The symbol $O\uparrow$ on the right-hand side of the above reaction indicates oxygen, without specifying either the exact form of the diffusing species (atom, cation, molecule), or its location (dislocation, pore).

As already mentioned above, in order for metal to precipitate within the oxide lattice, MgO structural units must be removed to create the necessary space for the new phase. Above a critical precipitate size, the compressive elastic strain energy stored in the surrounding oxide matrix becomes larger than a threshold value (of the order of the theoretical shear strength of MgO) and free dislocations are created in the oxide lattice. From this point on, plastic deformation can accommodate the deformation due to metal growth, and in this case $O\uparrow$ in Equation 2 could describe pipe diffusion of oxygen along dislocation lines. As a matter of fact, no dislocations could be found around very small precipitates at both reaction temperatures (see Figs 5 and 8), while the larger precipitates were always surrounded by a rather large number of dislocations.

To emphasize the extent of the stresses created by the reduction reaction, let us once again consider Equation 2. The point-defect cluster ($V_{cat}'' + V_{an}^{x} + 2h^{\cdot}$) can be visualized as a structural hole in the oxide matrix, the volume of which is close to that of an MgO lattice molecule. Reduced nickel can precipitate as metal in this empty space. If we compare the lattice constants of MgO, that is, of the structural hole of Equation 2 (neglecting the relaxation effects, 0.422 nm) with the lattice constant of nickel (0.358 nm), it becomes clear that, due to the large difference in volume of the two phases, internal reduction could theoretically result in a state of substantial tension of the surrounding matrix. This tension would be released if about every third vacancy pair was used for other purposes than providing the necessary space for the growing particle, for example, for dislocation climb or loop formation. These structural holes unused for the precipitation of the metal phase could also

account for the isolated pores locally observed in our samples.

The direct substitution of one MgO lattice molecule by one metal atom of nickel automatically yields the topotactic orientation relationship ($[0\,0\,1]_{MgO} \parallel [0\,0\,1]_{Ni}$ and $(1\,0\,0)_{MgO} \parallel (1\,0\,0)_{Ni}$), where all lattice planes of the two phases are parallel, as observed in our experiments.

A final comment should be made about our observations that, at low temperature, reduction yields small precipitates and a mostly dislocation-free matrix, while at high temperatures both small and large precipitates form, as well as an extensive dislocation network. A first explanation could be that, at low temperatures, where the bulk kinetics are still very slow, Ostwald ripening did not occur extensively during our experiments. As a consequence, the particles might be still below the critical size above which dislocations are formed. A second explanation could rely upon the difference in activation energy of the various slip systems in MgO: from the two slip systems, $\{1\,0\,0\}\ \langle 1\,1\,0\rangle$ and $\{1\,1\,0\}\ \langle 1\,1\,0\rangle$, only the second one is activated at temperatures lower than about 1673 K [12].

We finally want to mention the presence of small loops, 50 to 100 nm in diameter (rarely, some of these loops reach 600 nm in diameter), in our samples reduced at low temperature (Fig. 8). Since they cannot be found around every precipitate, but only around certain ones, they might have been present in the starting material, as the result of the quenching of the original crystal after its growth. Loops of this type can form during cooling around small impurity precipitates or atoms, as a result of the different thermal expansion coefficients. However, since the loops in Fig. 8 always enclose particles somewhat larger in size than those located outside the loop, we believe that the loops form during the reduction. They would allow a (limited) oxygen transport and therefore a faster growth of the nearby precipitates.

5. Conclusion

In the present paper, we have shown that the microstructure developed by internal reduction of (Mg, Ni)O varies strongly with temperature. In particular, at 1673 K the precipitates are larger and surrounded by dislocations, whereas at 1273 K they remain small and no free dislocations can be observed in their vicinity. The orientation relationship between oxide and metal lattices is found to be exclusively $[0\,0\,1]_{MgO} \parallel [0\,0\,1]_{Ni}$ and $(1\,0\,0)_{MgO} \parallel (1\,0\,0)_{Ni}$, which can be accounted for by a kinetic model where a nickel atom directly replaces a lattice molecule of MgO.

Our model predicts that from the initial stages of metal precipitation (coherent particles) onwards, the oxide matrix is set under compressive stresses. Above a threshold value of these stresses, dislocations form in the oxide matrix and plastic deformation can contribute to relaxing further stress build-up. At the newly-formed dislocations, the reduction reaction can be described as the formation of free oxygen, which then diffuses along the dislocation pipes to the outer surface, and of pairs of vacancies corresponding to missing lattice molecules in the oxide phase. The vacancy pairs provide the necessary space for the precipitating metal phase, and contribute to dislocation climb and pore growth. Whether or not free dislocations form is likely to depend on the temperature at which the reduction takes place, through such parameters as the activation energy of MgO slip systems, the kinetics of Ostwald ripening, or the kinetics of the reduction itself.

Acknowledgements

One of the authors (M.B.-R.) wants to thank the Deutsche Forschungsgemeinschaft for a fellowship which made this study possible. Financial support provided by the Volkswagen Foundation is gratefully acknowledged. The transmission electron microscopes were made available to us by the Institut für Metallphysik in Göttingen, the Max Planck Institut für Werkstoffkunde in Stuttgart, and the Materials Science Center of Cornell University. Furthermore, both authors want to thank Professor H. Schmalzried for helpful discussions.

References

1. C. WAGNER, *Z. Elektrochem.* **63** (1959) 772.
2. H. SCHMALZRIED, *Ber. Bunsenges. Phys. Chem.* **87** (1983) 551.
3. *Idem, ibid.* **88** (1984) 1186.
4. D. RICOULT and H. SCHMALZRIED, *J. Mater. Sci.* **22** (1987) 2257.
5. *Idem, J. Phys. Chem. Minerals* in press.
6. G. HONJO and K. YAGI, "Current Topics in Materials Science, Vol 6 (1980).
7. K. M. OSTYN and C. B. CARTER, *Surf. Sci.* **121** (1982) 360.
8. P. K. DAVIS and J. MACKINNON, *J. Amer. Ceram. Soc.* **69** (1986) C124.
9. J. NARAYAN, Y. CHEN, R. M. CHEN and R. W. CARPENTER, *Phil. Mag. A* **49** (1984) 287.
10. J. NARAYAN and Y. CHEN, *ibid.* **49** (1984) 475.
11. H. SCHMALZRIED, *React. Solids* **1** (1986) 117.
12. T. BRETHEAU, J. CASTAING, J. RABIER and P. VEYSSIERE, *Adv. Phys.* **28** (1979) 829.

Received 30 April
and accepted 6 July 1987